Nuclear Instruments and Methods in Physics Research B 90 (1994) 330–338
North-Holland

NIM B
Beam Interactions with Materials & Atoms

Effects induced by high electronic excitations in pure metals: a detailed study in iron +

A. Dunlop *, D. Lesueur, P. Legrand and H. Dammak
CEA / DTA / CEREM / DTM, Laboratoire des Solides Irradiés, Ecole Polytechnique, 91128 Palaiseau Cedex, France

J. Dural
Centre Interdisciplinaire de Recherche avec les Ions Lourds, BP 5133, 14040 Caen Cedex, France

Although high electronic excitations were neglected for a long time in radiation effect studies of metallic targets, it is now well established that they can play a dominant role in the damaging processes of some metals. Iron is especially interesting in so far as, according to the rate of energy deposition in electronic excitations $(dE/dx)_e$, various behaviours are observed. Below $(dE/dx)_e \approx$ 40 keV/nm, due to electronic excitations, the amount of damage introduced in the sample is smaller than that expected from the sole elastic collisions. On the contrary, at very high $(dE/dx)_e$ levels, a strong enhancement of the damage occurs. After describing the experimental results obtained during low temperature irradiations with a few 10 MeV/nucleon heavy (oxygen to uranium) ions, a phenomenological model which accounts for this intricate behaviour will be presented. Finally, a microscopic mechanism will be proposed to explain how the energy given to the electronic system can play a role in damage processes involving atomic motion. Molecular dynamics simulations validate this approach.

1. Introduction

In the frame of a systematic study of high electronic excitation effects in crystalline pure metals, particular attention was given to the case of iron, as the study of defect creation is made easier due to the high thermal stability of point defects (stage I migration occurs at ≈ 90 K). This paper will give an overview of all the results relative to GeV heavy ion irradiations of iron. Some of them have been previously published [1–3].

During the last few years, it has been well established that high levels of linear energy deposition in electronic excitations (usually referred to as LET) during swift heavy ion irradiations can induce structural modifications in metallic systems, such as point defect creation, phase transformation or even latent track formation (for a review see ref. [4]). Thus, metals and insulators do not behave so differently, although the LET thresholds above which damage occurs differ by at least one order of magnitude. The use of GeV heavy ions allows (i) to reach sufficient LET levels (typically ≥ 40 keV/nm) to damage metals and (ii) to minimize the relative contribution of elastic collisions to damage creation. In the usual experimental conditions, the ratio between the linear rates of energy deposition in electronic and nuclear collisions stays greater than ≈ 1000.

After a short presentation of the experimental setup and results, the various behaviour observed according to the LET level are discussed. A phenomenological model accounts for the experimental observations. Moreover, a microscopic model based on the Coulomb explosion mechanism is proposed to describe the elementary process allowing a conversion of part of the energy lost in electronic excitation into atomic displacements. Such an approach is confirmed by molecular dynamics simulations.

2. Experimental

High-purity iron ribbons (see ref. [2] for detailed impurity content) were cold-rolled to thicknesses of 3 to 15 μm, annealed at 500–800°C under 1.5 atm of purified hydrogen for 24 h. Their residual resistivity ratios, $\rho_{300\,K}/\rho_{4\,K}$, were typically of the order of 200.

In order to vary the LET level in the same irradiation, such ribbons are piled up perpendicularly to the ion beam. The total thickness of the stack is always much smaller than the projected range of the projectile, so that the stopping region of the ions is carefully

* Corresponding author. tel. +331 69334494, fax +331 69333022.
+ Irradiations performed in the GANIL accelerator in Caen (France).

SSDI 0168-583X(93)E1109-Y

avoided. These piled-up samples are introduced in a liquid helium cryostat. Actually the temperature of the samples is maintained close to 15 K, which implies a limitation of the incident ion flux to a few 10^8 ions/cm^{2}s. At such a low temperature, no thermal migration of irradiation induced defects is possible in iron.

In each sample, taking into account the slowing-down of the ions in the cryostat window, gaseous helium and preceding samples, it is easy to evaluate the average energy E of the ions, their average LET $[=(\mathrm{d}E/\mathrm{d}x)_e]$ and the cross-section σ_n [2] for elastic collisions which are all reported in Table 1. Using swift oxygen to uranium ions allows one to cover a wide LET range going from 1 to 70 keV/nm as can be seen in Fig. 1 where points representative of the various irradiations are reported.

The kinetics of damage creation is followed by in-situ electrical resistance measurements performed during beam stops. At the end of each irradiation up to fluences Φ_{max} (quoted in Table 1), isochronal annealing up to 250 K is performed: after heating up the

Table 1
Summary of the main experimental characteristics and extracted physical parameters defined in the text. The upper part of the table corresponds to the low LET region (region I), whereas the lower part is relative to the high LET region (region II)

Sample [a]	Ion	E [GeV]	$(\mathrm{d}E/\mathrm{d}x)_e$ [keV/nm]	η	σ_n [$\times 10^{-16}$ cm^2]	Φ_{max} [$\times 10^{12}$ cm^{-2}]	$\Delta\rho\,(\Phi_{max})$ [$\mu\Omega$ cm]	σ_d [$\times 10^{-16}$ cm^2]	σ_r [$\times 10^{-16}$ cm^2]	% ann. (150 K)	$T_{1/2}$ [keV]
O1-1	^{16}O	0.18	1.32	0.38	0.0056	110	0.046	0.0037	–	70	1.6
O1-2	^{16}O	0.096	2.02	0.51	0.0099	110	0.053	0.0046	–	68	1.8
Ar1	^{36}Ar	0.35	6.75	0.86	0.032	43	0.060	0.013	–	55	1.4
Kr1-1	^{84}Kr	2.34	11.3	1.03	0.040	5.8	0.010	0.017	–	–	2.2
Kr1-2	^{84}Kr	1.97	12.6	1.10	0.046	5.8	0.012	0.019	–	–	2.7
Kr1-3	^{84}Kr	1.32	16.0	1.29	0.067	5.8	0.022	0.027	–	–	3.0
Kr2-1	^{84}Kr	2.36	11.3	1.03	0.040	14	0.025	0.015	–	52	2.2
Kr2-2	^{84}Kr	1.99	12.5	1.10	0.045	14	0.027	0.017	–	48	2.7
Kr2-3	^{84}Kr	1.35	15.9	1.28	0.066	14	0.042	0.023	–	38	3.0
Kr2-4	^{84}Kr	0.60	21.6	1.68	0.142	14	0.055	0.043	–	35	3.9
Kr2-5	^{84}Kr	0.22	24.8	2.14	0.342	14	0.082	0.078	–	40	7.7
Xe1-1	^{129}Xe	2.81	25.2	1.60	0.102	11.6	0.041	0.028	–	31	4.6
Xe1-2	^{129}Xe	2.81	25.2	1.60	0.102	11.6	0.036	0.025	–	37	4.6
Xe1-3	^{129}Xe	2.37	28.2	1.69	0.114	11.6	0.045	0.031	–	36	5.8
Xe1-4	^{129}Xe	1.92	29.6	1.81	0.142	11.6	0.048	0.033	–	–	5.6
Xe1-5	^{129}Xe	1.44	32.6	1.98	0.189	11.6	0.055	0.038	–	36	5.7
Xe1-6	^{129}Xe	0.97	36.0	2.19	0.264	11.6	0.063	0.044	–	33	8.9
Xe1-7	^{129}Xe	0.57	38.3	2.46	0.429	11.6	0.086	0.059	–	34	10.5
Xe1-8	^{129}Xe	0.57	38.3	2.46	0.429	11.6	0.077	0.053	–	33	10.5
Xe2	^{129}Xe	4.68	19.2	1.32	0.062	18.5	0.044	0.022	–	40	4.0
Pb1-1	^{208}Pb	4.43	4.71	2.21	0.203	24	0.122	0.081	610	31	
Pb1-2	^{208}Pb	4.18	48.0	2.25	0.207	24	0.125	0.085	630	31	
Pb1-3	^{208}Pb	3.35	51.5	2.39	0.253	3.5	0.049	0.15	–	–	
U1-1 *	^{238}U	2.63	64.3	2.82	0.463	3.9	0.204	0.69	1940	–	
U1-2 *	^{238}U	2.25	65.8	2.91	0.520	3.9	0.214	0.74	2070	–	
U1-3 *	^{238}U	1.77	67.1	3.05	0.637	3.9	0.275	1.06	2790	–	
U1-4 *	^{238}U	1.35	67.8	3.19	0.836	3.9	0.317	1.39	3680	–	
U1-5 *	^{238}U	1.00	67.4	3.34	1.057	3.9	0.391	1.78	4070	–	
U1-6 *	^{238}U	0.75	65.8	3.47	1.297	3.9	0.535	2.71	4810	–	
U2-1	^{238}U	4.00	58.7	2.55	0.316	11.4	0.180	0.29	930	40	
U2-2	^{238}U	2.70	64.1	2.80	0.456	11.4	0.460	0.83	2400	38	
U3-1	^{238}U	4.61	56.6	2.46	0.271	0.5	0.010	0.16	–	37	
U3-2	^{238}U	2.75	63.9	2.79	0.451	0.5	0.029	0.47	–	43	
U3-3	^{238}U	2.62	64.4	2.82	0.463	0.5	0.033	0.57	–	44	
U3-4	^{238}U	1.65	67.6	3.09	0.719	0.5	0.063	1.15	–	43	
U4-1	^{238}U	4.45	56.7	2.49	0.271	3.36	0.052	0.17	1960	40	
U4-2	^{238}U	2.32	65.5	2.89	0.487	3.36	0.166	0.63	2790	40	
U4-3	^{238}U	0.97	67.1	3.36	1.080	3.36	0.414	2.08	4790	35	

[a] All experiments were performed at a temperature lower than 15 K on the GANIL accelerator in Caen (France) except those quoted by (*) which were performed at ≈ 90 K on the GSI accelerator in Darmstadt (Germany).

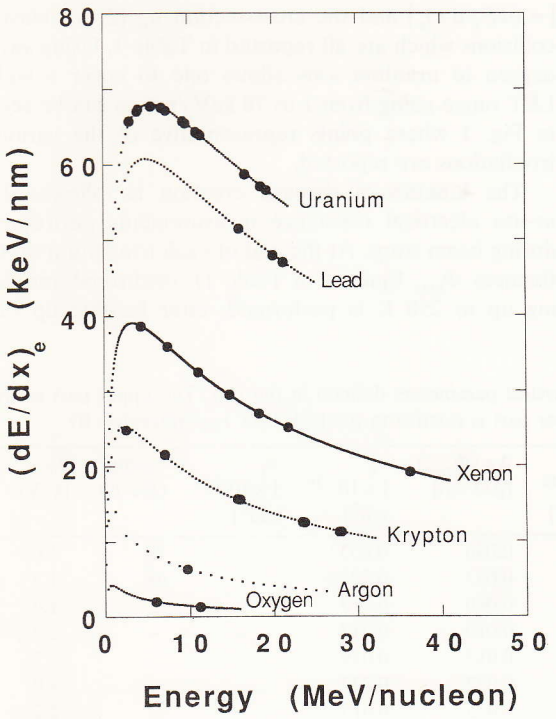

Fig. 1. Linear rate of energy deposition in electronic excitation of different projectiles in iron targets as a function of the projectile energy. Each experiment is indicated by a full circle.

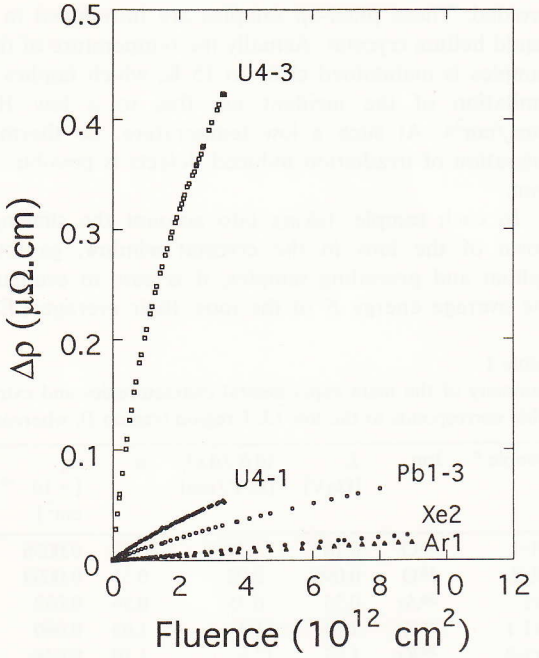

Fig. 2. Electrical resistivity variations at 15 K as a function of the ion fluence of iron targets for various irradiations: 0.35 GeV Ar, 4.68 GeV Xe, 3.35 GeV Pb, 4.45 and 0.97 GeV U.

samples during 10 min at increasing temperatures, the electrical resistances of the samples are measured at 15 K in order to evaluate the proportion of irradiation defects which have disappeared. Electron microscopy observations at 300 K have then been performed on some samples.

3. Results

3.1. Damage production

Some typical damage production curves are presented in Fig. 2. Strong contradictions appear if the following assumptions are made:

(i) As usually admitted, the electrical resistivity increase, $\Delta\rho$, is proportional to the defect concentration c ($\Delta\rho = c\rho_F$, in which ρ_F is the Frenkel pair resistivity), so that the experimental cross-section σ_d for damage production is defined by $\Delta\dot{\rho}_0 = (d\,\Delta\rho/d\Phi)_{\Phi=0} = \sigma_d\rho_F$.

(ii) Damage results only from elastic collisions (which implies $\sigma_d = \sigma_n$).

For instance, comparing the results relative to Ar1, Xe2 and U4-3 samples, it is obvious that:

– Ar1 and Xe2 curves are almost superimposed, whereas the elastic cross-sections σ_n differ by a factor of 2 (Table 1);

– The rate of variation of U4-3 curves is about 100 times greater than that of Xe2, although the corresponding σ_n differ by a factor of ≈ 17.

These inconsistencies cannot be ascribed to hypothesis (i) above. In the energy range considered here, the cross-sections for elastic collisions follow a Rutherford law [5] which favours low energy transfers, so that most of the defects are isolated. A rough estimation gives an average number of displaced atoms per primary knock-on atom smaller than 10 and a mean free path between two primary collisions greater than 100 nm.

Hypothesis (ii) has thus to be ruled out: elastic collisions alone cannot account for the experimental evidences. A convenient way to evidence the relative contribution of inelastic collisions to the measured damage is to normalize the observed damage rate to that expected from nuclear collisions. An efficiency, ξ, is defined by $\xi = \sigma_d/\sigma_n$. The cross-sections, σ_n, for defect production in elastic collisions (see Table 1) have all been calculated using a displacement threshold energy $E_d = 25$ eV by integrating the integral equations of Lindhard et al. [6], governing radiation damage, which were slightly modified [2].

It has to be noticed that the *absolute* values of ξ depend on the Frenkel-pair resistivity ρ_F used in the normalisation: among all the published values for iron, $\rho_F = 1250$ $\mu\Omega$ cm [7] has been retained here. This choice of ρ_F is unimportant as long as one intends to correlate ξ with inelastic processes. The most straightforward parameter characterizing the inelastic collisions is the LET level. Fig. 3 shows that ξ and $(dE/dx)_e$ are rather well correlated. Two regimes appear clearly: (i) in region I below 40 keV/nm, the efficiency decreases monotonically, whereas (ii) in region II above 40 keV/nm a spectacular increase of ξ is observed.

3.2. Damage annealing

Fig. 4 shows the evolution of the percentage of recovery of the electrical resistivity as a function of the annealing temperature for a few typical irradiations.

After irradiation with oxygen ions (low LET level), the annealing behaviour is very close to that observed after MeV electron irradiation [8]. As the LET level increases in region I, the amount of annealing decreases continuously, whereas in region II at high LET levels the annealing starts increasing again. This behaviour is more obvious in Fig. 5, where the amount of annealing at the end of stage I (≈ 150 K) has been plotted as a function of the LET level for all irradiated and annealed samples.

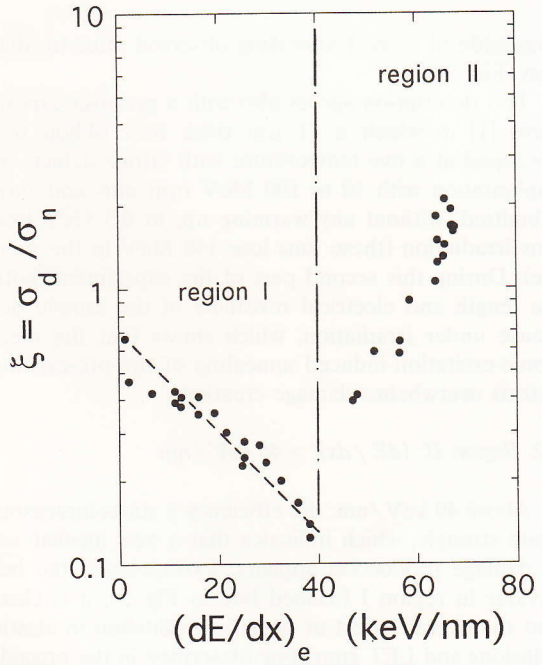

Fig. 3. Semi-logarithmic plot of the evolution of the damage efficiency, ξ, as a function of the LET level.

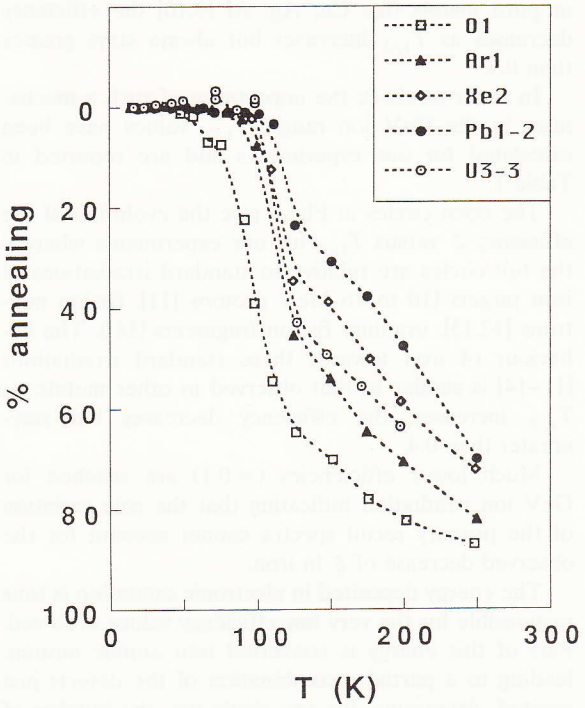

Fig. 4. Some typical ten minute isochronal recovery curves of heavy ion irradiated iron.

4. Discussion

The two LET regimes mentioned in section 3.1 will now be discussed separately.

4.1. Region I: $(dE/dx)_e < 40$ keV/nm

Let us recall that when the LET level increases, both the efficiency, ξ, and the amplitude of stage I recovery decrease, which can be interpreted as a partial recovery during the irradiation of the defects resulting from elastic collisions.

Efficiency values much smaller than 1 were also found during irradiations of various metals with a few 100 keV ions. When the mass of the projectile increases, i.e. when the primary recoil spectra becomes harder, the measured efficiency decreases gradually from about 1 to values as low as 0.3–0.4 [9,10]. In order to characterize the recoil spectra, a median recoil energy $T_{1/2}$ (such that half of the defects created in the target are due to displacements induced by primaries of energies $T > T_{1/2}$) has been defined. A good correlation between ξ and $T_{1/2}$ was then established:

in pure metals like Cu, Ag, Al [9,10] the efficiency decreases as $T_{1/2}$ increases but always stays greater than 0.3.

In order to check the importance of such a mechanism in the GeV ion range, $T_{1/2}$ values have been calculated for our experiments and are reported in Table 1.

The open circles in Fig. 6 give the evolution of the efficiency ξ versus $T_{1/2}$ for our experiments whereas the full circles are relative to standard irradiations of iron targets (10 to 16 MeV protons [11], fission neutrons [12,13], uranium fission fragments [14]). The behaviour of iron towards these standard irradiations [11–14] is similar to that observed in other metals: as $T_{1/2}$ increases, the efficiency decreases but stays greater than 0.4.

Much lower efficiencies (≈ 0.1) are reached for GeV ion irradiation indicating that the sole variation of the primary recoil spectra cannot account for the observed decrease of ξ in iron.

The energy deposited in electronic excitation is thus responsible for the very low efficiency values observed. Part of this energy is converted into atomic motion, leading to a partial recombination of the defects just created, decreasing, for one single ion, the number of produced defects. This is consistent with the small amplitude of stage I annealing observed after irradiation (Fig. 5).

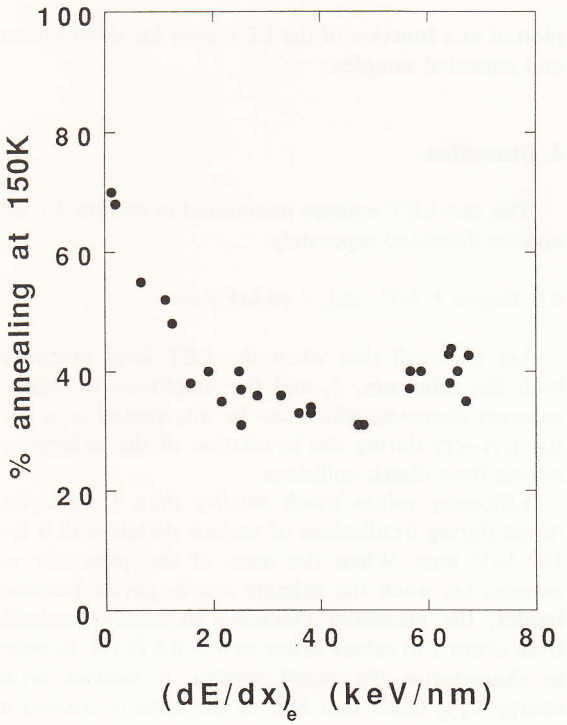

Fig. 5. Percentage of annealing at the end of stage I (≈ 150 K) as a function of the LET level after 15 K irradiations of iron with swift heavy ions.

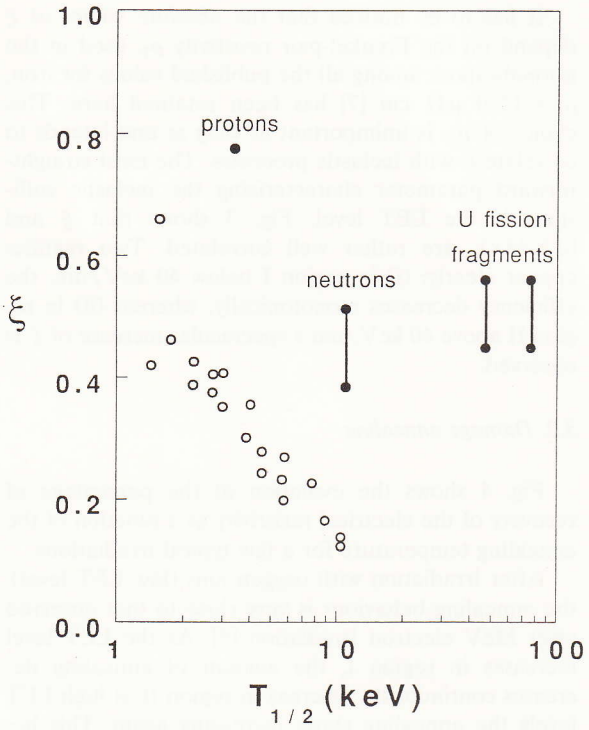

Fig. 6. Damage creation efficiency, ξ, as a function of the energy, $T_{1/2}$, characterizing the primary spectra (see text) for our experiments (open circles) and for MeV protons [11], fission neutrons [12,13] and uranium fission fragments [14] (full circles).

This description agrees also with a previous experiment [1] in which a 11 μm thick iron ribbon was predoped at a low temperature with lattice defects by implantation with 10 to 100 MeV iron ions and *then* submitted, without any warming up, to 0.5 GeV iron ions irradiation (these ions lose 140 MeV in the sample). During this second part of the experiment, both the length and electrical resistivity of the sample decrease under irradiation, which shows that the electronic-excitation-induced annealing of the pre-existing defects overwhelms damage creation.

4.2. Region II: $(dE/dx)_e > 40$ keV/nm

Above 40 keV/nm, the efficiency ξ starts increasing again strongly, which indicates that a new mechanism of damage production appears. Extrapolating the behaviour in region I (dashed line in Fig. 3), it is clear that the overall effect of damage production in elastic collisions and LET annealing (described in the preceding section) becomes completely negligible as compared to this new process of damage production. Thus,

the experimental cross-section, σ_d, is equal in region II to the cross-section, σ_e, of damage production by electronic excitation.

What is the structure of the damage created by this new process? A few indications suggest that one deals mainly with isolated point defects:

(i) The percentage of annealing in stage I starts increasing again slightly (Fig. 5).

(ii) No defect cluster could be seen by electron microscopy observations at 300 K. Moreover, a careful search of any hint indicating the appearance of a new phase (similarly to what was observed in irradiated titanium [15]) was unsuccessful.

5. Models describing damage production by electronic excitation

On the basis of the high density of very mobile conduction electrons, the possibility of damaging a metal by electronic excitation might appear very puzzling.

The energy deposition in electronic excitations is mainly restricted to the vicinity close to the ion path, so that an inhomogeneous repartition of the damage can be expected. Based on this remark, a phenomenological model describing the kinetics of damage production is presented in section 5.1. A possible elementary mechanism accounting for the conversion of this energy into atomic displacements is proposed in section 5.2, and validated by molecular dynamics calculations presented in section 5.3.

5.1. A phenomenological model

The equation describing the evolution of the average concentration, $\bar{c}$, of the defects as a function of the ion fluence, Φ, must account for the various processes encountered above:

(i) damage production in elastic collisions, described by the cross-section σ_n;

(ii) self-annealing of this damage mainly due to the high LET levels, described by a cross-section σ_{s-a}, so that the net cross-section for damage creation is $\sigma_n^* = \sigma_n - \sigma_{s-a}$,

(iii) damage production by electronic excitation, described by the cross-section σ_e.

With these notations, $\bar{c}$ obeys the following equation:

$$\frac{d\bar{c}}{d\Phi} = (\sigma_n^* + \sigma_e)(1 - 2v_0\bar{c}), \tag{1}$$

which implies

$$\Delta\rho = \frac{\rho_F}{2v_0}\left[1 - \exp\left(-2v_0(\sigma_n^* + \sigma_e)\Phi\right)\right]. \tag{1a}$$

In these equations, v_0 is the spontaneous recombination volume (expressed in atomic volumes). A previous irradiation of iron with MeV electrons [17] allowed the determination of the ratio v_0/ρ_F (for $\rho_F = 1250$ $\mu\Omega$ cm this leads to $v_0 \approx 100$ atomic volumes). Eq. (1) is similar to that proposed by Dettmann et al. [16] to describe isolated point defect production during MeV electron irradiation. Let us recall that it was pointed out in section 4.2 that damage resulting from swift ion irradiation very likely consists of rather isolated point defects.

In region I, $\sigma_e \ll \sigma_n^*$, so that the initial damage production rate is $(d\bar{c}/d\Phi)_{\Phi=0} = \sigma_n^* = \sigma_d$ (Table 1). In the domain of available fluences, the experimental $\Delta\rho(\Phi)$ curves do not sufficiently deviate from linearity to test with any confidence the exponential law (1a).

In region II, $\sigma_n^* \ll \sigma_e$ (see section 4.2), so that the initial damage production rate is $(d\bar{c}/d\Phi)_{\Phi=0} = \sigma_e = \sigma_d$ (Table 1). Moreover, in most cases a marked curvature of the experimental damage production curves (some of which are reported in Fig. 2) is observed, which allows a tentative fit with the exponential law (1a). Unfortunately, such a fit was proved to be absolutely impossible due to the fact that both the initial slope and curvature of the experimental data could not be accounted for by the sole free parameter σ_e of Eq. (1a). More precisely, the curvature of the experimental data is much more pronounced than expected from (1a), which corresponds to a saturation resistivity increase lower than $\rho_F/2v_0$. Such a behaviour can be accounted for by the addition in the right-hand side of Eq. (1) of a recombination term $(-\sigma_r\bar{c})$ [16]. All the experimental curves can now be well fitted with

$$\frac{d\bar{c}}{d\Phi} = \sigma_e(1 - 2v_0\bar{c}) - \sigma_r\bar{c}, \tag{2}$$

$$\Delta\rho = \rho_F\frac{\sigma_e}{(\sigma_r + 2v_0\sigma_e)}\left[1 - \exp\left(-(\sigma_r + 2v_0\sigma_e)\Phi\right)\right]. \tag{2a}$$

The two adjustable parameters $\sigma_e(=\sigma_d)$ and σ_r have been reported in Table 1 and plotted versus $(dE/dx)_e$ in Fig. 7. It has to be noticed that the ratios $(\sigma_r/2v_0\sigma_e)$ are of the order of a few tens, so that the recombination term governs the kinetics of damage production.

The recombination cross-sections, σ_r, obtained for GeV ions are much higher, by almost eight orders of magnitude, than those corresponding to electron irradiation [17]. These large recombination cross-sections, σ_r, can be imaged as continuous cylinders, of diameters ranging from 2.5 to 10 nm, in which annealing of pre-existing defects takes places. Thus the overall repartition of the damage in the sample is very inhomogeneous: point defects are located in the close vicinity of the ion path, and are surrounded by large defect-free regions.

A more realistic scheme of the recombination process could be to suppose that the cylinder in which annealing occurs is not completely free of defects, i.e. contains some defect agglomerates. These defect agglomerates would give an additional contribution to the electrical resistivity, keeping in mind that the contribution per defect in an agglomerate is much smaller than ρ_F [18]. Such an approach was previously considered to account for damage production in Co, Zr and Ti irradiated with swift heavy ions [19]. Let us emphasize that this implies the introduction of two other parameters in the adjustment process.

In this work, the range of available fluences was too restricted to allow a single-valued reliable set of four parameters to be extracted from the fits.

5.2. A microscopic model

When a swift heavy ion penetrates a target, ionized atoms are formed in the close neighbourhood of its path and excited electrons are ejected [20].

Consideration of the energy carried away by these δ-electrons leads to a so called "thermal-spike" model. Such a model was invoked years ago for insulating materials [21]; more recently a tentative extension to metallic targets was published [22]. In this model, the kinetic energy of the electrons is converted into atomic vibrations via electron–phonon coupling. The resulting heating-up of the lattice might well account for the defect recombination and annealing described in this paper.

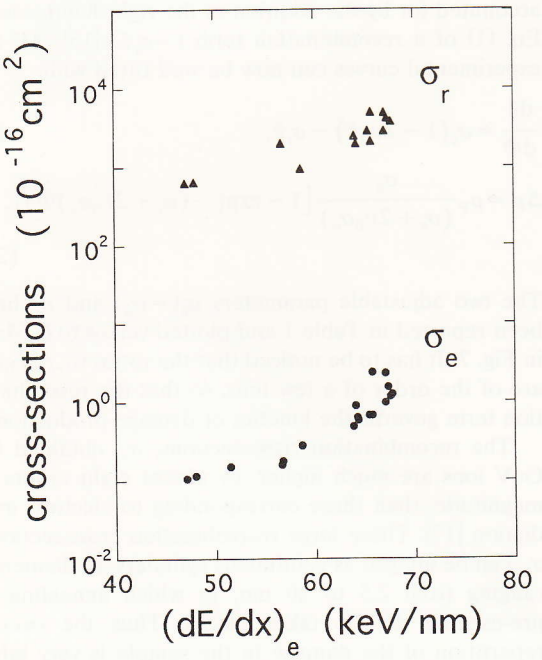

Fig. 7. Cross-section for damage creation (σ_e) and recombination (σ_r) by electronic processes as a function of the LET level.

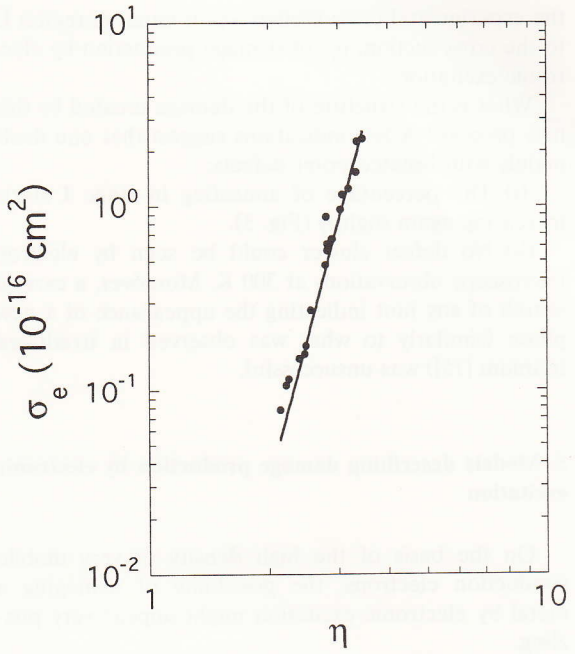

Fig. 8. Cross-section for damage creation (σ_e) by electronic processes as a function of the Coulomb explosion parameter, η. The continuous line corresponds to the η^8 law (see text).

Considering now the relaxation of the electrostatic potential energy stored in the space charge resulting from the ionization of the atoms leads to a Coulomb explosion model that was already used in insulators and organic materials [23]. Contrary to what happens in insulators, the lifetime of the space charge in a metal is extremely short, due to the presence of numerous free conduction electrons. This lifetime, τ, is roughly given by $\omega_p^{-1} \approx$ a few 10^{-16} s (ω_p is the plasma frequency). Nevertheless, for sufficiently high LET levels, when the ionization occurs inside a continuous cylinder, it has been shown [24] that the recoil energy, E_r, acquired by the ionized atoms due to Coulomb repulsion can reach 0.1 to a few eV.

As far as *individual* collisions are considered, recoil energies smaller than the threshold energy E_d (≈ 25 eV) cannot lead to defect creation. In such a scheme, Coulomb explosion appears to be inefficient towards damage creation. But, the *collective* and *coherent* aspects of the recoils have to be taken into account, so that the concept of threshold energy, E_d, becomes meaningless. In fact, it has been shown that the spatial and temporal coherence of these excitations allows an easy coupling to the phonon spectrum [25]. More precisely, low frequency modes are preferentially excited,

which occurs (i) for acoustic waves (i.e. $q \approx 0$) and (ii) for soft modes (usually at large q values) if any. In the first case, a radial shock-wave is generated, whereas in the latter large amplitude atomic movements are induced. Either of these two processes can lead to structural modifications and/or to defect creation.

Damage creation by electronic excitations is governed by the recoil energy, E_r. For a given target, E_r is related to the projectile characteristics by a unique parameter η, as detailed below. The space charge created along the ion path varies roughly as $(Z_1^*/v)^2$ [24], in which v is the ion velocity and $Z_1^*(v)$ the ion effective charge (which can be deduced from the Northcliffe formula [26]). Introducing a dimensionless parameter $\eta = Z_1^* v_0/v$ (v_0 is the Bohr velocity), the electric field resulting from the space charge varies as η^2, so that the ionized atoms receive during the lifetime τ impulses proportional to η^4 and acquire kinetic recoil energies $E_r \propto \eta^8$.

In the frame of this model, the pertinent parameter governing damage creation by electronic excitation should be the Coulomb explosion parameter, η, rather than the LET. The damage cross-section, σ_e, is reported in Fig. 8 as a function of η. This plot emphasizes a good correlation between σ_e and η. More precisely, σ_e is proportional to η^8, as indicated by the solid line in Fig. 8, which is in good agreement with the Coulomb explosion model.

Let us remark that the parameter η increases monotonically as the ion slows down, whereas the LET goes through a maximum. The points relative to irradiation U1 corresponding to LET levels located on both sides of the maximum are well aligned in Fig. 8, which shows that η appears as a better parameter than the LET to account for damage processes resulting from high levels of energy deposition by electronic excitation.

5.3. Molecular dynamics simulation

In order to test more quantitatively the ability of numerous collective and coherent low energy transfers to induce permanent lattice displacements, molecular dynamics simulations have been performed [27]. In a small perfect bcc, crystal containing about 6000 iron atoms thermalized at a temperature of 50 K, the Coulomb explosion has been simulated by imposing as initial conditions that all the atoms lying inside a cylinder of radius ≈ 10 Å receive the same radial outward kinetic energy E_r (which was varied in the range 0.5 to 2 eV/atom). The system relaxes then freely in the simulation box.

The potential used in these simulations is a new original N-body potential which reproduces well the phonon spectrum [27]. The position of all the atoms is followed during the relaxation of the system. When the system has lost the memory of the excitation (a few 10^{-12} s) and after using a damping procedure in order to stabilize the system, the new positions of lattice atoms have been examined in order to detect the possible presence of permanent lattice defects. As soon as the recoil energy E_r is higher than ≈ 1 eV, lattice defects are created (Fig. 9), with cross-sections of order of magnitude comparable with the measured damage cross-section σ_e. No influence of the incident ion beam direction with respect to crystallographic directions could clearly be put forward.

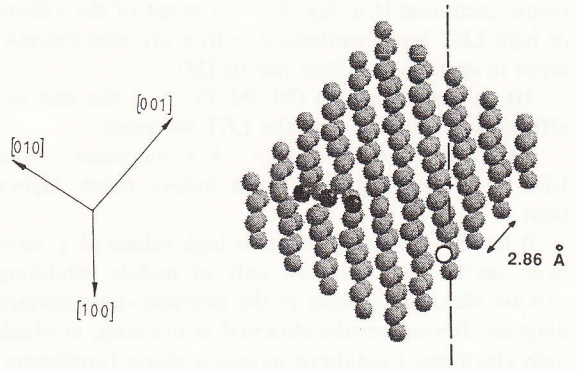

Fig. 9. Region of an iron crystallite in which lattice defects were detected after the passage on an ion along the [100] axis (its trajectory is represented by the dashed line). In this simulation, outward recoil energies of 1.16 eV/atom were given to atoms located inside a cylinder of radius 11.5 Å. The black spheres correspond to interstitial atoms, whereas the hollow sphere corresponds to a vacancy (from ref. [27]).

On the other hand, if in the same size cylinder, a Maxwellian distribution of recoil energies centered on the same value E_r is now applied but in random orientations, no defect creation could be detected. This emphasizes the crucial importance of the coherence of the excitation in the collective process of damage creation by electronic excitation.

Finally, it appeared interesting to check whether such a mechanism could also lead to the recombination of pre-existing defects. Starting now with a crystal in which a pre-existing stable Frenkel pair was introduced, it was shown that recoil energies as low as 0.2 eV/atom were sufficient to induce the recombination of this Frenkel pair lying in the vicinity of the ion path [27].

6. Conclusion

In this detailed study of iron targets, various aspects of the influence of high electronic excitation on the processes of damage production have been put forward. Although some metals are insensitive to elec-

tronic excitation (Cu, Ag, W, ···), some of the effects of high LET levels evidenced in iron are also encountered in quite a few other metals [28]:

(i) In certain metals (Ni, Pd, Pt, ···), the damage efficiency, ξ, decreases as the LET increases.

(ii) In others (Ti, Co, Zr, ···), ξ increases as the LET increases and can reach values much higher than 1.

It has been pointed out that high values of ξ have been up to now obtained only in metals exhibiting various allotropic phases in the pressure–temperature diagram. Recent results obtained in titanium, in which high electronic excitations induce a phase transformation from the usual hcp, α-phase towards the high-pressure hexagonal ω-phase [15], support the Coulomb explosion mechanism in which a radial high pressure shock-wave is generated. This phase change in titanium is only observed at the highest LET levels (≈ 40 keV/nm), whereas at lower LET levels (≈ 29 keV/nm) the observed damage could well be premonitory signs of the $\alpha \rightarrow \omega$ phase transformation. In the same way, the high values of ξ measured in Zr and Fe could well be related to the existence of high-pressure phases in these two metals.

Let us finally point out that although it is straighforward to scale electronic excitation effects with the linear rate of energy deposition $(\mathrm{d}E/\mathrm{d}x)_e$, the use of the Coulomb explosion parameter, η, is more pertinent. For a given target, this parameter depends only on the atomic number and velocity of the projectile. At very high velocities, $(\mathrm{d}E/\mathrm{d}x)_e$ is almost proportional to η^2, so that the use of either of these parameters to scale the effects is equivalent. On the contrary, at lower velocities, namely in the vicinity of the Bragg maximum, $(\mathrm{d}E/\mathrm{d}x)_e$ is not related to η in a straightforward way.

References

[1] A. Dunlop, D. Lesueur, G. Jaskierowicz and J. Schildknecht, Nucl. Instr. and Meth. B 36 (1989) 412.

[2] A. Dunlop, D. Lesueur and J. Dural, Nucl. Instr. and Meth. B 42 (1989) 182.

[3] A. Dunlop, D. Lesueur, J. Morillo, J. Dural, R. Spohr and J. Vetter, Nucl. Instr. and Meth. B 48 (1990) 419.

[4] A. Dunlop and D. Lesueur, Mater. Sci. Forum 97–99 (1992) 553.

[5] J. Lindhard, V. Nielsen and M. Scharff, K. Dan. Vidensk. Selsk. Mat. Fys. Medd. 36 (10) (1968).

[6] J. Lindhard, V. Nielsen, M. Scharff and P.V. Thomsen, K. Dan. Vidensk. Selsk. Mat. Fys. Medd. 33 (10) (1963).

[7] P.G. Lucasson and R.M. Walker, Phys. Rev. 127 (1962) 485.

[8] H. Bilger, V. Hivert, J. Verdone, J.L. Leveque and J.C. Soulie, Proc. Int. Conf. on Vacancies and Interstitials in Metals, Jülich, Germany, 1968, p. 751.

[9] R.S. Averback, R. Benedek, K.L. Merkle, J. Sprinkle and L.J. Thompson, J. Nucl. Mater. 113 (1983) 211.

[10] R.S. Averback, R. Benedek and K.L. Merkle, Phys. Rev. B 18 (1978) 4156.

[11] D.A. Thompson, A.M. Omar and J.E. Robinson, J. Nucl. Mater. 85–86 (1979) 509.

[12] A. Dunlop, B.M. Pande K. Böning, P. Rosner and H.E. Schäfer, J. Nucl. Mater. 108 (1982) 83.

[13] G. Wallner, M.S. Anand, L.R. Greenwood, M.A. Kirk, W. Mansel and W. Waschkowski, J. Nucl. Mater. 152 (1988) 146.

[14] A. Dunlop, N. Lorenzelli and W. Mansel, Nucl. Instr. and Meth. B 33 (1988) 706.

[15] H. Dammak, A. Barbu, A. Dunlop, D. Lesueur and N. Lorenzelli, Philos. Mag. Lett. 67 (1993) 253.

[16] K. Dettmann, G. Leibfried and K. Schröder, Phys. Status Solidi 22 (1967) 423.

[17] J. Dural, J. Ardonceau and J.C. Jousset, J. Phys. (Paris) 38 (1977) 1007.

[18] M. Asdente and J. Friedel, J. Phys. Chem. Solids 11 (1959) 115.

[19] H. Dammak, D. Lesueur, A. Dunlop, P. Legrand and J. Morillo, Radiat. Eff. Def. Solids 126 (1993) 111.

[20] R.L. Fleischer, P.B. Price and R.M. Walker, Nuclear Tracks in Solids: Principles and Applications (University of California Press, 1975).

[21] L.T. Chadderton and H. Montagu-Pollock, Proc. R. Soc. A 274 (1969) 239.

[22] M. Toulemonde, C. Dufour and E. Paumier, Phys. Rev. B 46 (1992) 14362.

[23] I.S. Bitensky and E.S. Parilis, Nucl. Instr. and Meth. B 21 (1987) 26.

[24] D. Lesueur and A. Dunlop, Radiat. Eff. Def. Solids 126 (1993) 163.

[25] A. Dunlop, P. Legrand, D. Lesueur, N. Lorenzelli, J. Morillo, A. Barbu and S. Bouffard, Europhys. Lett. 15 (1991) 765.

[26] L.C. Northcliffe, Ann. Rev. Nucl. Sci. 13 (1963) 67.

[27] P. Legrand, J. Morillo and V. Pontikis, Radiat. Eff. Def. Solids 126 (1993) 151; P. Legrand, Thesis, CEA Rep. R-5639 (1993).

[28] A. Dunlop and D. Lesueur, Radiat. Eff. Def. Solids 126 (1993) 123.